# Essential Role for NFI-C/CTF Transcription-Replication Factor in Tooth Root Development

George Steele-Perkins,[1,2] Kenneth G. Butz,[1,2] Gary E. Lyons,[3] Margarita Zeichner-David,[4]
Heung-Joong Kim,[5] Moon-Il Cho,[5] and Richard M. Gronostajski[1,2,6]*

*Lerner Research Institute, Department of Cancer Biology, Cleveland Clinic Foundation,[1] and Department of Biochemistry,
Case Western Reserve University,[6] Cleveland, Ohio; Department of Anatomy, University of Wisconsin
Medical School, Madison, Wisconsin[3]; Center for Craniofacial Molecular Biology, University of
Southern California School of Dentistry, Los Angeles, California[4]; and Department of
Oral Biology, School of Dental Medicine,[5] and Department of Biochemistry,
School of Medicine and Biomedical Sciences,[2] State University of
New York at Buffalo, Buffalo, New York*

The mammalian tooth forms by a series of reciprocal epithelial-mesenchymal interactions. Although several signaling pathways and transcription factors have been implicated in regulating molar crown development, relatively little is known about the regulation of root development. Four genes encoding nuclear factor I (NFI) transcription-replication proteins are present in the mouse genome: *Nfia*, *Nfib*, *Nfic*, and *Nfix*. In order to elucidate its physiological role(s), we disrupted the *Nfic* gene in mice. Heterozygous animals appear normal, whereas *Nfic*$^{-/-}$ mice have unique tooth pathologies: molars lacking roots, thin and brittle mandibular incisors, and weakened abnormal maxillary incisors. Feeding in *Nfic*$^{-/-}$ mice is impaired, resulting in severe runting and premature death of mice reared on standard laboratory chow. However, a soft-dough diet mitigates the feeding impairment and maintains viability. Although *Nfic* is expressed in many organ systems, including the developing tooth, the tooth root development defects were the prominent phenotype. Indeed, molar crown development is normal, and well-nourished *Nfic*$^{-/-}$ animals are fertile and can live as long as their wild-type littermates. The *Nfic* mutation is the first mutation described that affects primarily tooth root formation and should greatly aid our understanding of postnatal tooth development.

---

Tooth formation is a complex developmental process that is mediated through a series of epithelial-mesenchymal interactions (29). Several signaling pathways required for early molar tooth development have been identified, including the BMP (31), FGF (13, 27), SHH (5, 10), and WNT (25, 33) pathways. In addition, targeted disruption of a number of transcription factors, including *Msx1* and *-2* (1), *Dlx1* and *-2* (22), *Pax-9* (21) and others, severely disrupts early tooth development. In contrast, only one pathway regulating late tooth developement has been identified. The Tabby (*Ta*), Downless (*Dl*), and Crinkled (*Cr*) mouse mutations each cause similar defects of postnatal development (32) by disrupting different components of the Ectodysplasin-A hormone signaling system.

The nuclear factor I (NFI) family of transcription-replication factors is encoded by four genes in mammals (NFI-A, -B, -C, and -X) and a single gene in *Drosophila melanogaster* and *Caenorhabditis elegans* (8, 14, 23). Prokaryotic homologues of the NFI genes have not been identified. NFI was discovered as a protein required for adenovirus DNA replication in vitro (19, 20), but it is now clear that NFI proteins play an important role in the expression of many cellular genes (reviewed in reference 8). NFI-C/CTF was the initial NFI gene cloned (24) and contains a prototypical proline-rich transcriptional activation

domain, as well as a heptamer repeat homologous to the C-terminal domain of RNA polymerase II (18). Because products of the four NFI genes are often coexpressed (3) and bind to similar DNA sequences (15), it has been difficult to determine the roles of individual NFI family members in gene expression during development. We are analyzing the role of NFI genes in mouse development by generating mice deficient in each of the four NFI genes.

We disrupted the *Nfic* gene in mice by removal of its second exon, which encodes the NFI-C/CTF DNA-binding and dimerization domain. The most striking defect in *Nfic*$^{-/-}$ mice is that their molar teeth form no roots. In addition, their mature mandibular incisors are thin and brittle, and their maxillary incisors are dysmorphic. Consistent with these tooth defects, *Nfic*$^{-/-}$ mice exhibit compromised feeding on standard lab chow, resulting in increased morbidity and mortality. Since loss of *Nfic* is the first mouse mutation to specifically affect root development, these mice should be an important tool for understanding the molecular pathways essential for this process.

## MATERIALS AND METHODS

**Gene targeting.** Mouse genomic clones containing *Nfic* exon 2 were isolated from a mouse 129/Sv phage library as described previously (7). Endonuclease restriction, Southern blotting, PCR, and DNA sequencing were used to characterize clones, including mapping restriction sites and mapping and sequencing exons 1 and 2. The targeting vector contains 9.5- and 3.5-kb regions of 5′ and 3′ homology, respectively, flanking a PGK-Neo-bGHpA gene cassette (26) in the reverse transcriptional orientation. The Neo cassette replaces ~1.3 kb of *Nfic* from an *Nde*I site 98 bp 5′ of exon 2 to an *Nhe*I site ~700 bp 3′ of exon 2. The negatively selectable gene cassette MCI-TK (herpes simplex virus thymidine

* Corresponding author. Mailing address: Department of Biochemistry, School of Medicine and Biomedical Sciences, State University of New York at Buffalo, 140 Farber Hall, 3435 Main St., Buffalo, NY 14214. Phone: (716) 829-3471. Fax: (716) 829-2725. E-mail: rgron@buffalo.edu.

kinase with a mutant polyomavirus enhancer [17]) was adjacent to the shorter region of *Nfic* homology in the opposite transcriptional orientation. A total of $5 \times 10^6$ E14-1 mouse embryonic stem (ES) cells (12) were electroporated with 5 µg of *Xho*I-linearized targeting vector and then selected in 0.2 mg/ml of G418 (Gibco-BRL) and 2 µM ganciclovir (Roche Laboratories) for 6 days. Colonies were isolated and expanded twice in 96-well plates. Two plates were cryopreserved, and two were used for DNA isolation and Southern blot analyses.

**PCR genotyping.** Toe or 0.5-cm tail-tip biopsies were shaken at 55°C overnight in 0.5 ml of tail lysis buffer (0.05 M Tris-Cl, pH 8.0; 0.1 M EDTA; 0.5% sodium dodecyl sulfate), including 0.5 mg of proteinase K/ml. Then, 1 µl of the lysate diluted 1:25 in $H_2O$ was analyzed in 20-µl multiplex PCRs (2.5 U of platinum *Taq* DNA polymerase (Gibco-BRL), 1.5 mM $MgCl_2$, 0.2 mM concentrations of each deoxynucleoside triphosphate, 1× Rediload (Research Genetics), 1× PCR buffer (supplied with the *Taq*), and five primers at 0.2 µM each). The following two *Nfic*-specific primers (*a* and *c*), Neo-specific primer (*b*), and two mouse Y chromosome-specific primers (*SRY*) were used: *a* (5′-CATCTGTGTGAAACA GTCTGG-3′), *b* (5′-CCGCTTCCTCGTGCTTTACGG-3′), *c* (5′-AGCAGCTC ATCCTTCACCGCG-3′), *SRY1* (5′-AACAACTGGGCTTTGCACATTG-3′), and *SRY2* (5′-GTTTATCAGGGTTTCTCTCTAGC-3′). PCR products were resolved on 2.5% agarose gels and visualized with ethidium bromide.

**RT-PCR.** Total RNA was isolated by using TRIzol reagent (Gibco-BRL) according to the manufacturer's instructions. RNA from mandible was purified over a G50 spin column (Roche) prior to reverse transcription (RT). cDNA was generated from 2 to 5 µg of RNA by using Superscript (Gibco-BRL) according to the manufacturer's random-prime protocol. A total of 1 µl of each RT product was analyzed by PCR with a sense primer from exon 1 (5′-GATCGGCCTCAC GGGCCGATGTATTCCTCCCCGCTCTGC-3′) and an antisense primer from exon 3 (5′-TTGCTGTCCTCCTGGTCTGAGC-3′). Products were resolved on 2.5% agarose gels. Analysis of *Nfia*, *Nfib*, *Nfix*, amelogenin, ameloblastin, dentin sialophosphoprotein (DSPP), and $\beta_2$-microglobulin transcript levels was done by real-time quantitative PCR with an ABI 7700 or Bio-Rad real-time thermocycler with SYBRgreen detection. The primer sequences and conditions are available upon request.

**Mouse rearing.** The initial 17 F1 litters were fed a diet of autoclaved mouse chow (Purina 5010 and, for breeders, Purina 5021) and autoclaved distilled water. For studies requiring adults, several grams of the soft transgenic dough diet (S3472; Bio-Serv) were added to cages twice per week beginning 3 days prior to the P21 wean.

**Histology and in situ hybridization.** Postnatal mice were anesthetized with isoflurane and cardiac perfused with 4% paraformaldehyde–phosphate-buffered saline (PBS). Heads were removed and depelted, the craniums were evacuated, and the skulls were decalcified by soaking them in formaldehyde-formic acid at 4°C overnight. After paraffin embedding, 4-µm sections were cut and stained with hematoxylin and eosin (H&E). For embryos, fixing, embedding, sectioning, and in situ hybridization with $^{35}S$-labeled *Nfic* cRNA sense and antisense probes were performed as described previously (3, 16). The control sense probe shows a low background level of silver grains (not shown). For postnatal tissue in situ hybridizations, digoxigenin (DIG)-labeled *Nfic* sense and antisense cRNA probes were prepared by using the T7/Sp6 DIG RNA labeling kit (Roche). Sections were deparaffinized and hybridized according to the manufacturer's protocol. Briefly, sections were hydrated, treated for 20 min with proteinase K (20 µg/ml), washed with PBS, fixed in 4% paraformaldehyde, washed again in PBS, incubated with 0.2 N HCl for 10 min to inhibit endogenous alkaline phosphatase, and acetylated by incubation for 10 min in 0.1 M triethanolamine containing 0.25% acetic anhydride. After a washing step, hybridization was performed overnight at 50°C in hybridization solution (50% deionized formide, 10% dextran sulfate, 1× Denhardt solution, 4× SSC [1× SSC is 0.15 M NaCl plus 0.015 M sodium citrate], 10 mM dithiothreitol, 1 mg of yeast tRNA/ml, 1 mg of salmon sperm DNA/ml) containing the DIG-UTP-labeled *Nfic* cRNA sense or antisense probes. After being washed for 30 min with 2× SSC–50% formamide and 10 min each in 2× SSC and 0.2× SSC at 50°C, sections were incubated for 30 min with blocking solution, followed by incubation for 1 h with blocking solution containing 1:500 sheep anti-DIG-alkaline phosphatase Fab fragments. After being washed, DIG probes were detected by incubating the sections with alkaline phosphatase substrates (368 µg of nitroblue tetrazolium salt and 184 µg of BCIP (5-bromo-4-chloro-3-indolylphosphate) in 1 ml of 100 mM Tris-HCl, 100 mM NaCl, and 50 mM $MgCl_2$) until the color was developed. Sections were then used directly or counterstained for 2 to 3 min with methyl green, air dried, and mounted by using VectaMount (Vector Laboratories).

**Skull bones and molar teeth isolation.** Mouse heads were depelted, the muscles and fascia were clipped away, and the brains and eyes were removed before soaking the heads in 1% KOH for 3 days. After three rinses with $H_2O$, the heads were individually incubated in 50 mM Tris-Cl (pH 8.0), 0.5% SDS, and 0.2 mg of proteinase K/ml at 55°C for 20 min and then washed with $H_2O$. Molars of $Nfic^{-/-}$ mice separated from the jaw during proteolysis, whereas those of the other *Nfic* genotypes were isolated by crown extraction or fracturing the mandible or maxilla.

## RESULTS

***Nfic* gene targeting and confirmation of *Nfic*-null allele.** We constructed a replacement-type targeting vector substituting *Nfic* exon 2 with a neomycin resistance gene that is constitutively transcribed in the reverse direction (*Neo* in Fig. 1A). Since both the DNA-binding and the dimerization activities of NFI-C reside in exon 2, homologous recombination of the native gene and the targeting vector should yield a *Nfic*-null allele. On Southern blots an *Nfic* probe external to the targeting vector detects a 3.7-kb band from the targeted allele and a 9.5-kb band from the native allele on *Eco*RI digests of genomic DNA (the two thickest bars in Fig. 1A). A screen of 90 G418+ganciclovir-resistant ES clones identified four that harbored a targeted mutation and a composite of the results of the screen is shown (Fig. 1B).

We injected three *Nfic* heterozygous (+/−) ES clones into C57BL/6 blastocysts in order to generate mouse chimeras. Male chimeras were crossed to Black Swiss, 129S6, and C57BL/6 strains and genomic DNA from tail biopsies of progeny was screened by PCR for the presence of the mutated allele (data not shown). All three ES clones transmitted the mutated allele into the germ line. $Nfic^{+/-}$ mice were crossed and the progenies' genotypes were identified by PCR (Fig. 1C). The single PCR distinguishes both genotype and sex. Primers *a* and *c* amplify 358 bp of the native gene, whereas primers *a* and *b* amplify 545 bp of the targeted allele. Primers *SRY1* and *2* amplify ~150 bp of the Y chromosome. Southern blot analysis of these same DNAs confirmed the PCR results (data not shown).

To show that the targeted *Nfic* allele was null, we analyzed *Nfic* transcripts from brain and liver RNA of adult littermates of each *Nfic* genotype. Total RNA was isolated, reverse transcribed, and the cDNA was used as a template in PCRs with *Nfic* exon 1-specific (forward) and exon 3-specific (reverse) primers (Fig. 1D). As predicted, the PCR produced a single 638-bp product from brain and liver cDNA of the wild-type (+/+) mouse. This product is from a transcript that includes exon 2 (532 bp) and the termini of exons 1 and 3 (Fig. 1D, lanes +/+). The PCR generated two products from brain and liver cDNA of the $Nfic^{+/-}$ littermate (Fig. 1D, lanes +/−). The larger product corresponds to the wild-type transcript, whereas the smaller product corresponds to a 106-bp product resulting from a direct splice of exon 1 to 3. Only the smaller product was amplified from brain and liver cDNA of the $Nfic^{-/-}$ littermate (Fig. 1D, lanes −/−). Sequencing of the smaller product confirmed that it is generated from a direct splice from exon 1 to exon 3 (data not shown). Because the exon 1-exon 3 splice junction is out of frame, these aberrantly spliced *Nfic* transcripts are predicted to encode a 31-amino-acid missense polypeptide that terminates in exon 3.

**Viability, growth, and fertility of $Nfic^{-/-}$ mice.** Our initial 17 heterozygote crosses produced 154 F1 progeny distributed in a Mendelian ratio: 33 wild-type (21.4%), 87 $Nfic^{+/-}$ (56.5%), and 34 $Nfic^{-/-}$ mice (22.1%). We noted in early litters that
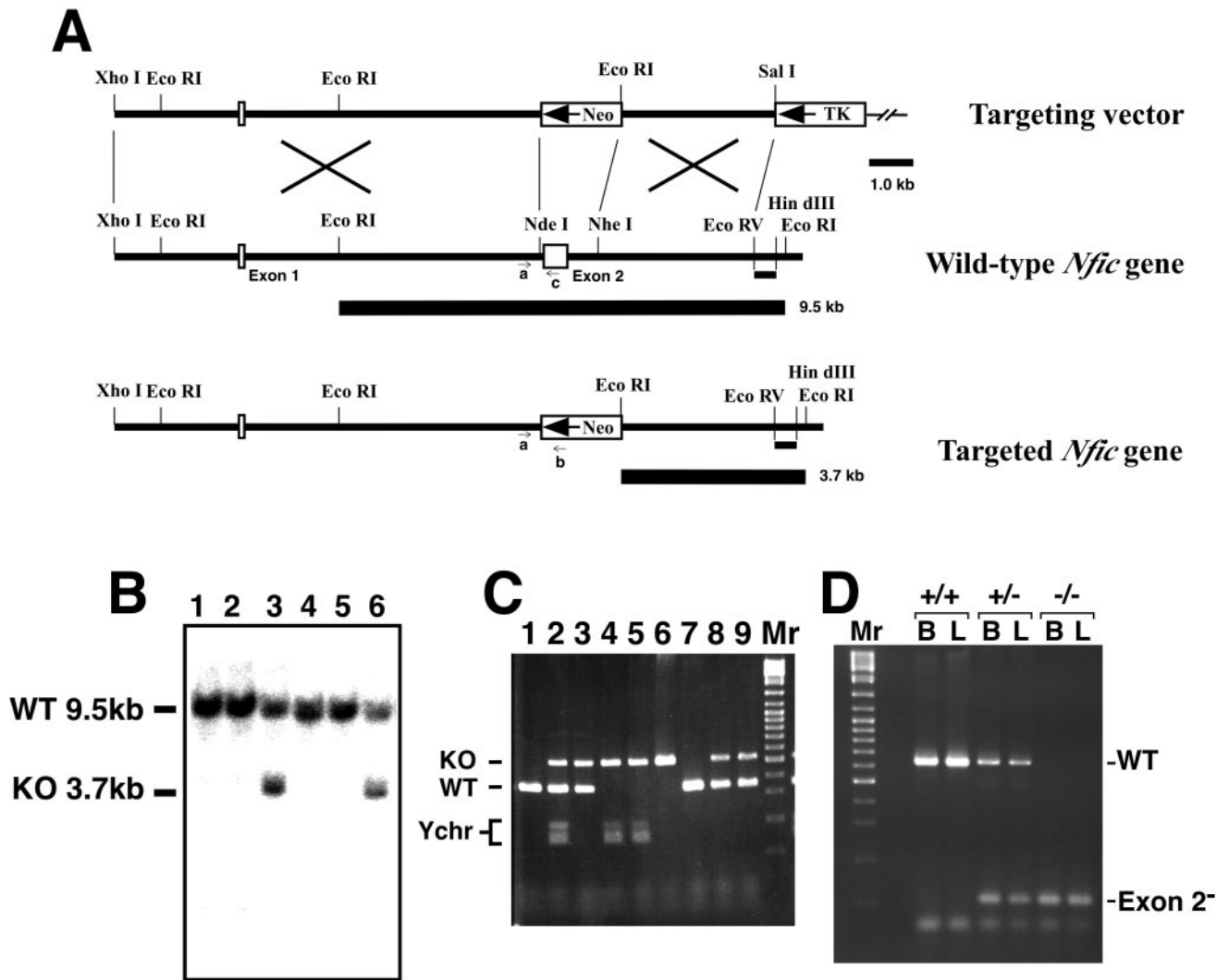
FIG. 1. Targeted mutation of the mouse *Nfic* gene. (A) Targeting vector (top), the *Nfic* region encompassing exons 1 and 2 (middle), and their homologous recombination product (bottom). The termini of homologous sequences and relevant restriction sites are noted. The positive and negative selection gene expression cassettes are boxes labeled Neo and TK, respectively, and their transcription orientations are indicated by arrows. Exons are indicated by open boxes labeled Exon. The 3′-flanking probe (*Eco*RV-*Hin*dIII; short bar) and the wild-type and mutant *Eco*RI restriction fragments it identifies in Southern analyses (thick bars) are shown. Plasmid backbone sequences are denoted by a thin line. Locations of the three primers (*a*, *b*, and *c*) used for PCR genotyping are indicated by small arrows. (B) Data from Southern blot screen of G418- and ganciclovir-resistant ES clones. Each of six clones is numbered above, and the hybridizing wild-type (WT 9.5kb) and mutant (KO 3.7kb) *Eco*RI fragments are indicated on the left. Clones 3 and 6 have a targeted mutation, whereas clones 1, 2, 4, and 5 do not. (C) PCR genotyping of one litter from an *Nfic* heterozygous cross. PCRs employing the three primers indicated in panel A plus two Y-chromosome-specific primers were used to screen tail biopsies of a litter of nine (lanes 1 to 9). Labels on the left indicate the 545-bp targeted-gene product (KO), the 358-bp wild-type product (WT), and the male-specific products (Ychr). Lanes (lane/progeny, *Nfic* genotype, sex): 1, +/+, female; 2, +/−, male; 3, +/−, female; 4, −/−, male; 5, −/−, male; 6, −/−, female; 7, +/+, female; 8, +/−, female; 9, +/−, female. Lane Mr is a 100-bp DNA ladder. (D) RT-PCR analysis of *Nfic* transcripts in tissues of each *Nfic* genotype. The total RNA isolated from brains (lanes B) or livers (lanes L) of *Nfic* wild-type (+/+), heterozygote (+/−), and homozygote (−/−) male P193 littermates was reverse transcribed, and the cDNA was then analyzed by PCR with exon 1- and exon 3-specific primers. The products corresponding to wild-type (WT) and aberrant (Exon 2⁻) transcripts are indicated. Lane Mr is a 100-bp DNA ladder.

postweaning *Nfic*⁻/⁻ mice became severely runted compared to their wild-type or *Nfic*⁺/⁻ littermates (Fig. 2A). Continued rearing of *Nfic*⁻/⁻ mice on standard lab chow resulted in continued runting and premature death (Fig. 2B and data not shown). Upon discovery of tooth defects in the *Nfic*⁻/⁻ mice (see below, Fig. 3 to 6), we added a soft-dough dietary supplement 3 days prior to weaning and continued the diet supplementation of *Nfic*⁻/⁻ mice postweaning. The dough diet sup-

plementation allowed all (*n* = 18) *Nfic*⁻/⁻ mice to survive longer than 3 months and into adulthood. Of three male and four female healthy adult *Nfic*⁻/⁻ mice bred with *Nfic*⁺/⁻ partners, all but one female mated successfully. The resulting litters were of normal size, the *Nfic* genotype ratio was the expected 1:1 (*Nfic*⁺/⁻:*Nfic*⁻/⁻), and the litters were reared successfully. These data indicate that *Nfic*⁻/⁻ mice have greatly increased morbidity and mortality when fed standard lab chow
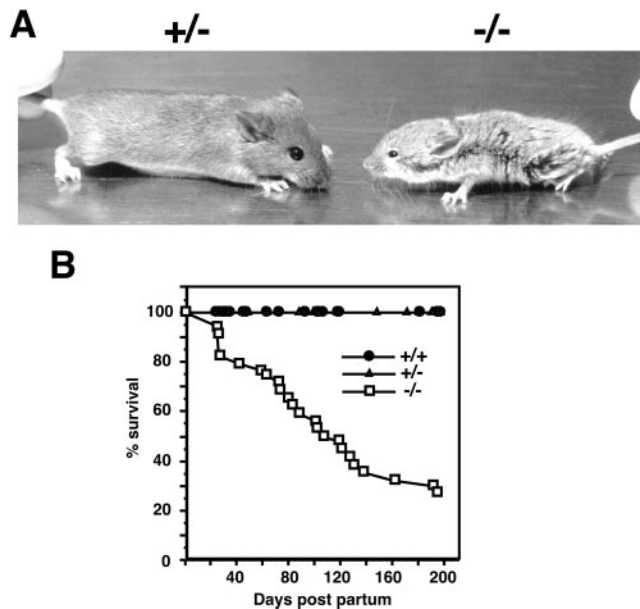
FIG. 2. Growth retardation and increased mortality of $Nfic^{-/-}$ mice. (A) Female P54 $Nfic^{+/-}$ and $Nfic^{-/-}$ littermates. Note the severe runting of the $-/-$ animal. A mirror image is shown in order to present the $-/-$ sibling on the right. (B) Mortality of $Nfic$ mice reared on standard chow. The percent survival of $Nfic^{-/-}$ ($n = 34$), $Nfic^{+/-}$ ($n = 84$), and $Nfic^{+/+}$ ($n = 33$) mice are plotted versus time. The points of the $+/-$ and $+/+$ curves indicate the time of sacrifice of littermates of $Nfic^{-/-}$ animals that had died. These studies were performed prior to observing tooth defects in $Nfic^{-/-}$ animals. Also, the increased mortality of $Nfic^{-/-}$ animals was not observed if they are reared on a soft-dough diet (see Results).

and that a soft diet supplement rescues the mortality, permitting survival and fertility.

**Abnormal incisor development in $Nfic^{-/-}$ mice.** Gross observations of the mouth and jaw of $Nfic^{-/-}$ mice revealed virtually no mandibular (lower) incisors and overgrown, thin maxillary (upper) incisors (Fig. 3A). The structurally compromised incisors are most likely responsible for the morbidity and mortality of $Nfic^{-/-}$ mice reared on standard lab chow that was described above. H&E staining of coronal sections of adult mandibles indicated grossly abnormal mandibular incisor development (Fig. 3B versus C). The wild-type mandibular incisors had a normal structure consisting of an oval core of dentin with enamel deposition mainly on one surface (Fig. 3B). However, mandibular incisors in $Nfic^{-/-}$ mice were highly disorganized, frequently showing scattered pockets of differentiated tissue (Fig. 3C, arrowheads).

A similar analysis of coronal sections of maxillae revealed a less pronounced but clearly abnormal maxillary incisor development in $Nfic^{-/-}$ mice (Fig. 4). The maxillary incisors of wild-type (not shown) and $Nfic^{+/-}$ animals were substantially thicker than those of $Nfic^{-/-}$ mice (Fig. 4A versus B). The maxillary incisors of wild-type and heterozygous animals have dentin around the entire circumference and enamel on one surface (Fig. 4C [expanded in panel E]). In contrast, the maxillary incisors of $Nfic^{-/-}$ animals have near-normal labial dentin and enamel deposition but nearly absent lingual dentin deposition, leading to a grossly nonsymmetric structure (Fig. 4D [expanded in panel F]).
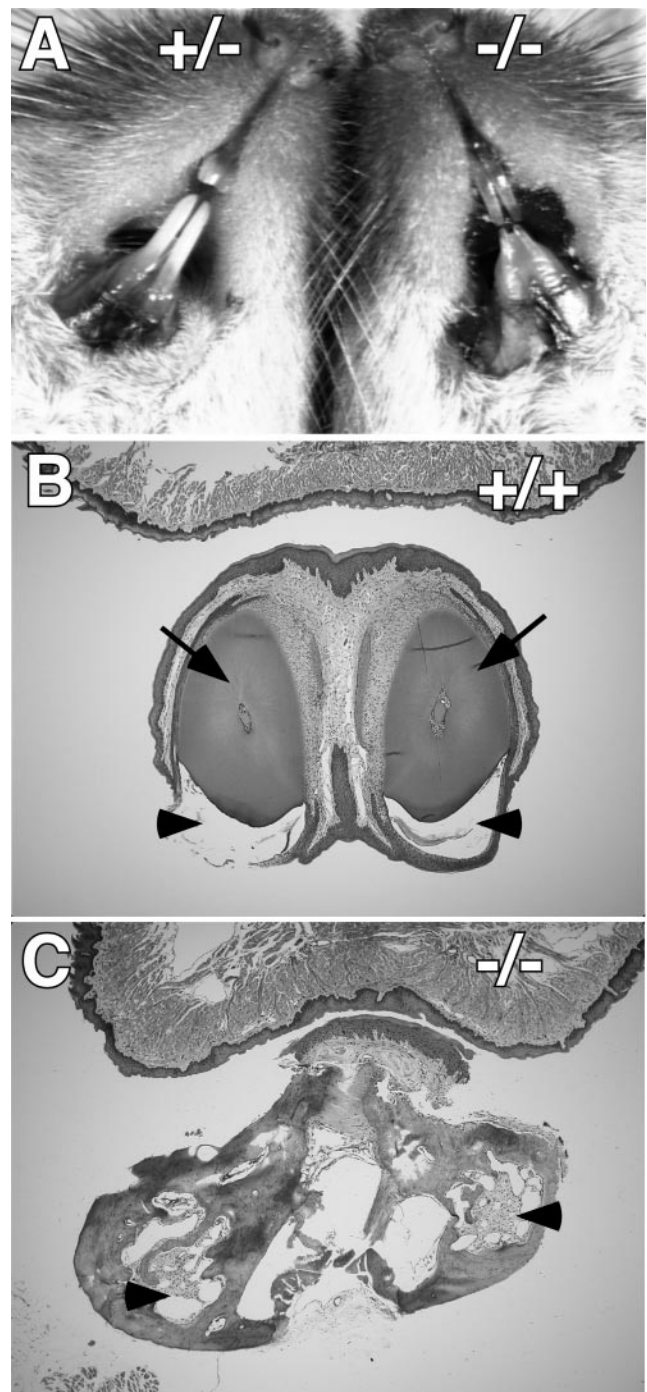


FIG. 3. Abnormal mandibular incisors of $Nfic^{-/-}$ mice. (A) View of mouths of two P40 female littermates ($Nfic^{+/-}$ and $Nfic^{-/-}$) reared on a soft-dough diet. Lower labia and tongues were excised to help expose incisors. Note the abnormally thin mandibular incisors and the extended gingiva of the $-/-$ animal. (B) Mandible portion of an H&E-stained coronal section of the jaw of an $Nfic^{+/+}$ P135 male. The tongue is at the top. An arrowhead and an arrow indicate the enamel and dentin, respectively. The majority of the enamel was lost during decalcification. (C) Same as panel B except the individual is a $Nfic^{-/-}$ littermate. Arrowheads indicate disorganized tissue where incisor structures are expected.
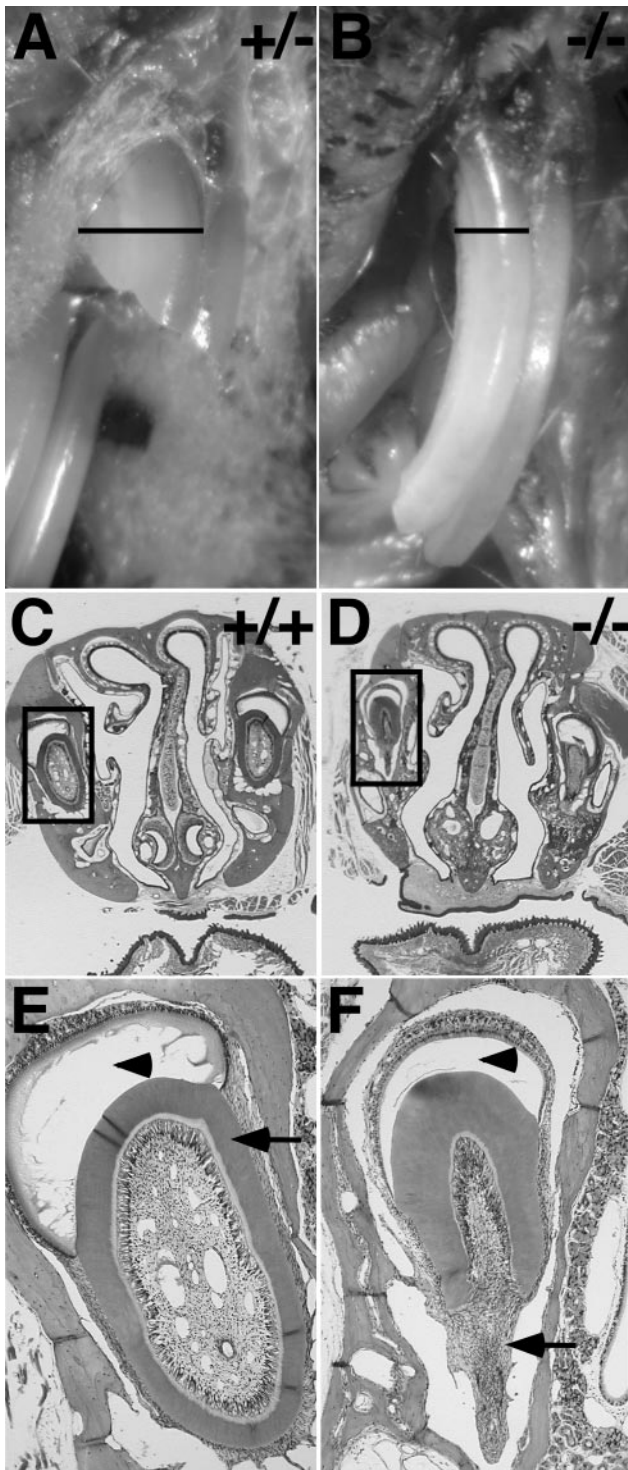
FIG. 4. Abnormal maxillary incisors of $Nfic^{-/-}$ mice. (A) Close view of maxillary incisors in situ of a P135 $Nfic^{+/-}$ male reared on standard chow. The black bar indicates thickness of the right maxillary incisor. (B) Same as panel A except the individual is an $Nfic^{-/-}$ littermate. Note that the incisor is thin compared to panel A. (C) Upper portion of an H&E-stained coronal section of the head of a P135 $Nfic^{+/+}$ male. The tongue is at the bottom. The box locates the right maxillary incisor. (D) Same as panel C except the individual is an $Nfic^{-/-}$ littermate. (E) Magnified view of boxed area in panel C. An arrowhead and an arrow indicate the enamel and dentin, respectively. Note the uniform layer of dentin around the circumference of the

**Abnormal molar root development in $Nfic^{-/-}$ mice.** To examine the structure and morphology of the molar teeth, we isolated first and second mandibular and maxillary molars from adult littermates. The molars of wild-type (not shown) and $Nfic^{+/-}$ mice had normal crowns and roots (Fig. 5A and C). The mandibular and maxillary molars had the appropriate two and three roots, respectively. In contrast, molars from $Nfic^{-/-}$ mice had normal crowns but no roots (Fig. 5B and D). The lack of roots was observed both bilaterally and in all $Nfic^{-/-}$ molars examined. In order to determine whether the molar roots of the adult $Nfic^{-/-}$ mice failed to form or were resorbed following development, we isolated molars from P15 littermates, an age at which roots are still forming. The molars of both wild-type and $Nfic^{-/-}$ P15 mice have normal-appearing crowns (Fig. 5E and F). In contrast, although the wild-type molars show immature roots extending from the base of the crown (Fig. 5E), $Nfic^{-/-}$ molars show no developing roots (Fig. 5F). To further confirm the failure of molar root formation, serial sagittal sections were taken through the mandibles of P14 mice. Again, wild-type molars show normal root development (Fig. 5G), whereas $Nfic^{-/-}$ molars show no root development (Fig. 5H). The histology reveals that the only apparent difference between wild-type and $Nfic^{-/-}$ mouse molar development is root formation. There appear to be no structural changes in the jaw that might impede root outgrowth. These data indicate that molar root formation in the $Nfic^{-/-}$ mouse fails at either the initial outgrowth of the epithelial sheath or during early extension of the root.

**Decreased alveolar (tooth socket) bone formation in $Nfic^{-/-}$ mice.** Since molar roots fail to form in $Nfic^{-/-}$ mice, we examined the jaw and the alveolar bone that normally surrounds the molar roots. Mandibles and maxillae of adult wild-type, $Nfic^{+/-}$ and $Nfic^{-/-}$ mice were prepared and examined by light microscopy. In the maxillae of both wild-type (not shown) and $Nfic^{+/-}$ mice, the incisors and molars remained embedded in bone during skull preparation (Fig. 6A). In contrast, the molars fell out during the preparation of $Nfic^{-/-}$ maxillae (Fig. 6A) and mandibles (Fig. 6D). Extraction of the molars from the maxillae of $Nfic^{+/-}$ animals revealed the deep root sockets of alveolar bone present in normal jaw (Fig. 6B). In contrast, the molar tooth sockets of $Nfic^{-/-}$ maxillae were shallow and contained an unorganized mesh of bony spicules (Fig. 6B). The mandible skeletons of $Nfic^{-/-}$ mice showed similar defects, both the incisors and molars detaching during preparation and the molar tooth sockets being filled with a coarse meshwork of alveolar bone (Fig. 6C and D and data not shown). In addition, the mandibles of $Nfic^{-/-}$ mice appear ~10% smaller than those of their wild-type and heterozygous littermates (Fig. 6D versus C). No such size difference was noted in maxillae (Fig. 6A).

To examine earlier stages of alveolar bone formation, we isolated skeletonized mandibles from P15 littermates. In contrast to what was seen with adult skulls, molars fell out of both +/+ and −/− mouse mandibles (Fig. 6E and F). At this age

incisor. (F) Magnified view of boxed area in panel D. An arrowhead indicates the enamel deposition at the labial side, whereas the arrow indicates the absence of dentin at the lingual side of the incisor.
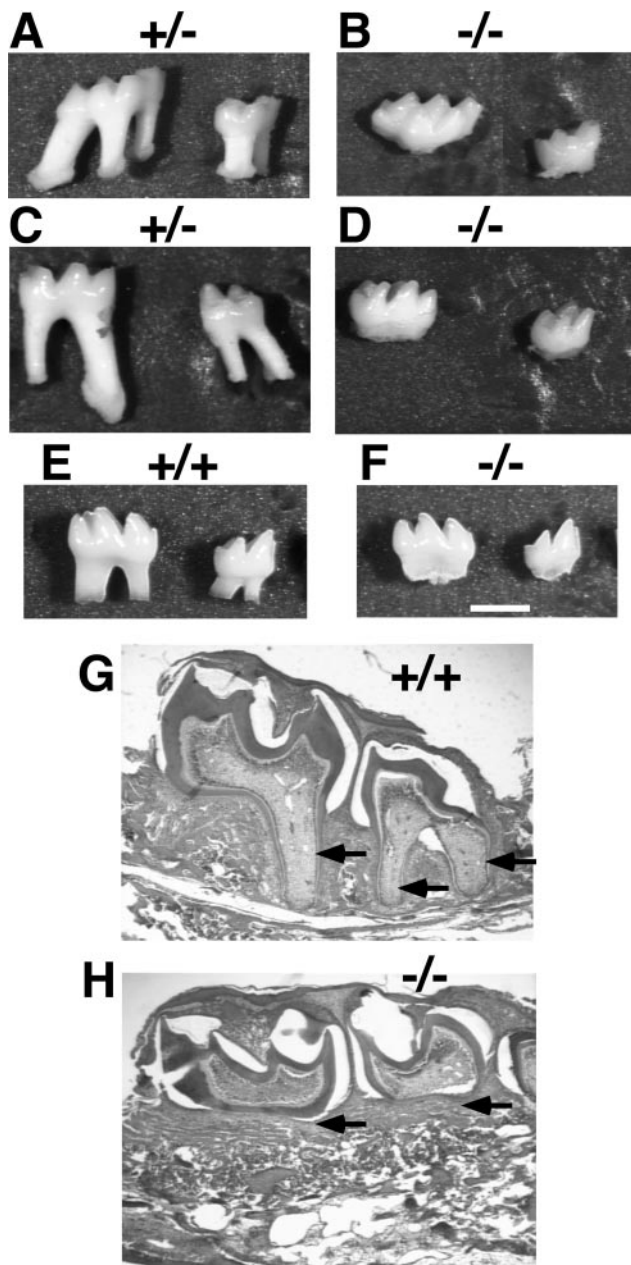
FIG. 5. Failure of molar root development in $Nfic^{-/-}$ mice. The panels compare the molars of P190 male (A to D), P15 male (E and F), and P14 male (G and H) littermates of the indicated $Nfic$ genotype. (A and C) Lateral views of first (left) and second maxillary (A) and mandibular (C) molars of a +/− mouse. (B and D) Lateral views of first (left) and second maxillary (B) and mandibular (D) molars of a −/− mouse. (E and F) Lateral views of first (left) and second (right) mandibular molars of +/+ (E) and −/− (F) littermates. Bar, 1 mm. (G and H) H&E-stained sagittal sections of the developing left mandibles of +/+ (G) and −/− (H) littermates. The perimeter of the immature first and second molars in each is demarcated by dark-staining dentin. Arrows denote the immature roots present in panel G but absent in panel H.

alveolar bone has begun to surround the emerging molar roots in +/+ mice, whereas no such bone formation is seen in the tooth sockets of −/− mice (Fig. 6F, +/+ versus −/−). In contrast, bone formation between the teeth appears similar in both +/+ and −/− animals (Fig. 6F, +/+ versus −/−).

**$Nfic$ expression during tooth development.** To assess when and where $Nfic$ is expressed during tooth development, we performed in situ hybridization with the $Nfic$-specific probe we described previously (3). During tooth bud development at E15.5, $Nfic$ is expressed strongly in the mesenchymal cells of the dental papilla and weakly in the epithelial components (Fig. 7A and B). When root formation is beginning at P8 (Fig. 7C), $Nfic$ is expressed strongly in most epithelial tissues of the tooth, including ameloblasts; in odontoblasts; in surrounding mesenchymal tissues, including the stellate reticulum; and in the dental papilla of the molars and incisor. No staining is seen with the control sense probe (Fig. 7D, F, and H). At P14, when molar root formation is in progress, $Nfic$ expression appears more restricted being present within the odontoblasts and pre-odontoblasts of the molars (Fig. 7E and G) and within the periodontal ligament and developing bone (Fig. 7G). Figure 7G and H are magnifications of the boxed regions of Fig. 7E and F, respectively. Thus, $Nfic$ is expressed at multiple stages of tooth development and strongly in odontoblasts and preodontoblasts during root formation.

**Decreased tooth-specific gene expression in $Nfic^{-/-}$ mice.** To determine whether the abnormal incisor and molar root development was reflected in changes in tooth-specific gene expression, we examined the levels of amelogenin, ameloblastin, and DSPP transcripts in RNA isolated from dissected P15 mandibles. Amelogenin (Amg) and ameloblastin (Amb) are expressed in ameloblasts, whereas DSPP is expressed in odontoblasts. Using real-time quantitative PCR, we found that levels of Amb, Amg, and DSPP were each reduced by >50% in mandibular RNA of $Nfic^{-/-}$ mice compared to their levels in heterozygous or wild-type mice (Fig. 8, lanes Amb, Amg, and DSPP). There were no consistent changes in transcript levels for α1 type I collagen in the $Nfic^{-/-}$ mice (Fig. 8, lane Col). These data are consistent with the histology of P15 $Nfic^{-/-}$ animals that show abnormal mandibular incisor and molar root development.

To assess whether the loss of $Nfic$ affected the expression of the other NFI genes, we measured $Nfia$, $Nfib$, and $Nfix$ transcript levels in mandibular RNA. No changes were detected in the transcript levels for the other three NFI genes in $Nfic^{-/-}$ mice (Fig. 8, lanes $Nfix$, $Nfib$, and $Nfia$). The levels of $Nfix$, $Nfib$, and $Nfia$ transcripts were also similar in liver RNA from wild-type and $Nfic^{-/-}$ mice (not shown). These data indicate that loss of $Nfic$ does not appear to affect the expression of the other NFI genes in the tissues examined.

## DISCUSSION

We show here that disruption of $Nfic$ causes major defects in postnatal murine tooth development, the most striking defect being loss of molar root formation (Fig. 5). In addition, there are clear defects in mandibular and maxillary incisor formation and in alveolar bone formation in molar tooth sockets (Fig. 3, 4, and 6). These tooth and bone defects cause runting and lethality unless the $Nfic^{-/-}$ animals are reared on a soft-dough diet (Fig. 2). Since $Nfic^{-/-}$ animals can survive and be fertile if maintained on nutrient dough, it appears that the tooth defects cause the lethal phenotype seen with loss of $Nfic$. Whether
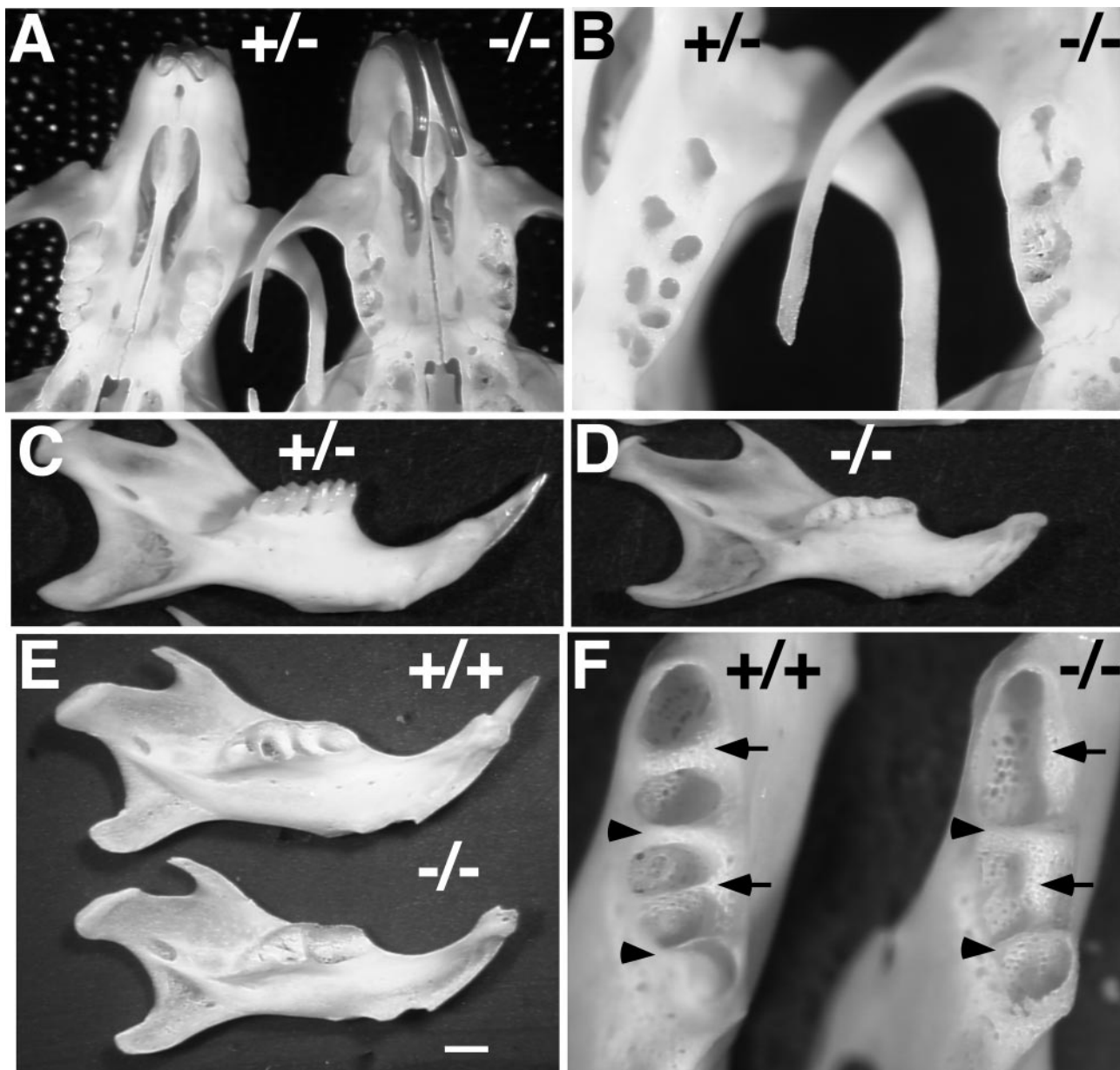
FIG. 6. Abnormal alveolar bone formation in *Nfic*$^{-/-}$ mice. (A) View of maxillae of skulls prepared from P97 male $+/-$ and $-/-$ littermates. (B) Closeup of molar root areas in center of panel A. Note that the $+/-$ mouse maxilla's left molars were extracted for the closeup, whereas the $-/-$ mouse molars dislodged during skull preparation. (C) Lingual view of left mandible of the same $+/-$ animal as in panel A. (D) Lingual view of left mandible of the same $-/-$ animal as in panel A. (E) Lingual view of left mandibles isolated from P15 male $+/+$ and $-/-$ littermates. Bar, 1 mm. (F) Closeup view of molar root sockets of mandibles shown in panel E. Both the $+/+$ and $-/-$ mouse mandibles are forming bone between the three molars (arrowheads). However, the $-/-$ mouse mandible is not forming bone at the regions between the missing roots of the first and second molars (arrows). The third molar of the $+/+$ mouse mandible did not dislodge during skull preparation (bottom).

additional nonlethal developmental defects are present in the *Nfic*$^{-/-}$ animals awaits further analyses.

The specific combination of defects seen in *Nfic*$^{-/-}$ mice (loss of molar roots with apparently normal crown formation and severe mandibular incisor disruption with milder maxillary incisor defects) is unique to this mouse and indicates a relatively late role for *Nfic* in tooth development. In contrast, loss of either *Msx-1* (1) or *Lef1* (33) causes the arrest of tooth development at the bud stage, which precludes analysis of late

events in tooth formation. Loss of both *Dlx-1* and *Dlx-2* results in complete agenesis of maxillary molars, whereas mandibular molars and incisors appear normal (22, 30). This differential effect of loss of the *Dlx* genes emphasizes the apparently unique molecular requirements of mandibular versus maxillary molar development. In addition, the lack of a dental phenotype in individual *Dlx* knockouts demonstrates the apparent redundancy of some transcription factors in maxillary molar development. Redundant functions in tooth formation have also
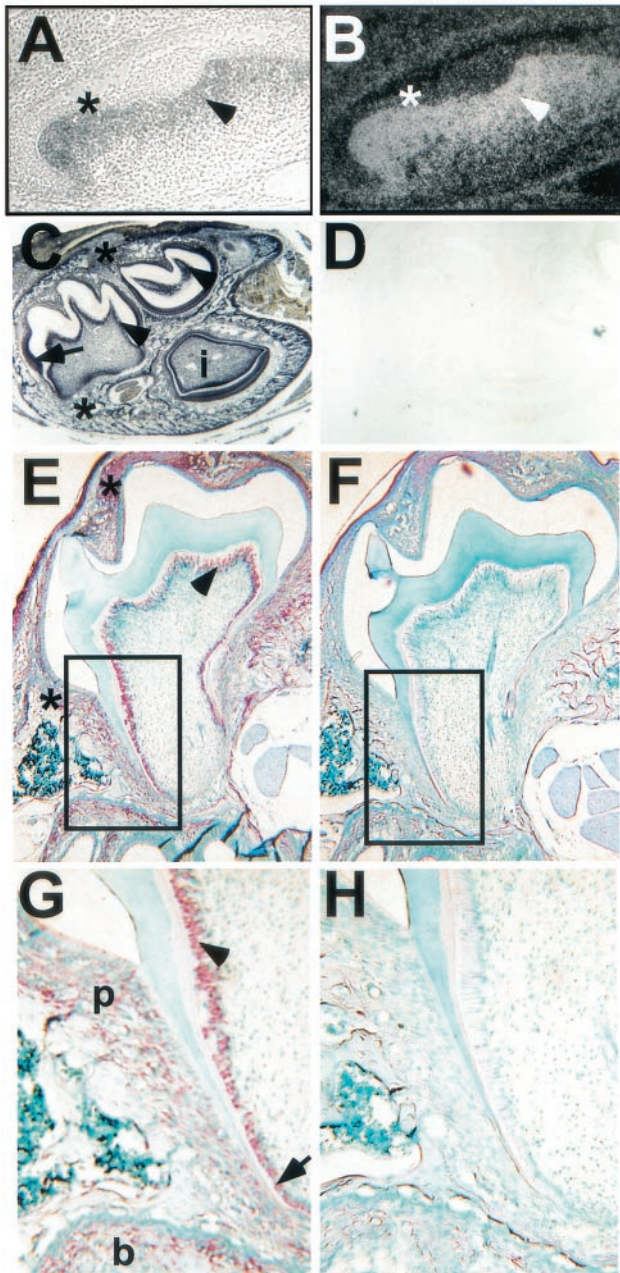
FIG. 7. *Nfic* expression during normal tooth development. *Nfic* expression was detected in wild-type animals by in situ hybridization using ^{35}S-labeled (A and B) and DIG-labeled (C to H) antisense (B, C, E, and G) and control sense (D, F, and H) *Nfic* probes. Panels A and B show phase-contrast and dark-field images, respectively, of an E15.5 mouse first maxillary molar hybridized with a ^{35}S-labeled *Nfic* antisense probe. Note the high *Nfic* expression in the molar mesenchymal cells (arrowhead), with weaker expression in the epithelium (asterisk). Panels C and D show staining by *Nfic* antisense and sense probes, respectively, of the mandible of a P8 mouse. Note the expression of *Nfic* in ameloblasts (arrow), odontoblasts (arrowheads), and surrounding connective tissue (top asterisk, stellate reticulum; bottom asterisk, mesenchymal tissues) and in the pulp of the molars and incisor (i) of panel C. No staining is seen with the control sense probe (D). Panels E and F show staining by *Nfic* antisense and control sense probes, respectively, in mouse P14 first maxillary molars. Sections were counterstained lightly with methyl green to identify cell types. *Nfic* is expressed in crown odontoblasts (arrow) and connective tissue (asterisks). Panels G and H are higher magnifications of panels E and F,
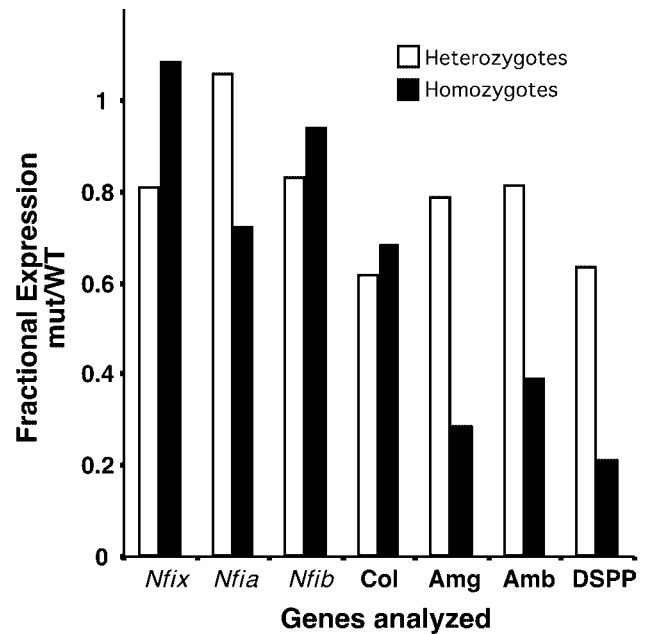


FIG. 8. Reduced tooth-specific gene expression in the mandibles of *Nfic*^{−/−} mice. *Nfix*, *Nfia*, *Nfib*, α1 type I collagen (col), amelogenin (Amg), ameloblastin (Amb), and DSPP transcript levels were quantified by real-time quantitative PCR and normalized to β$_2$-microglobulin levels in the same samples. The bars represent the average of three animals of each genotype. Values are expressed as the transcript levels found in heterozygous (white bars, +/−) and *Nfic*^{−/−} animals (black bars, −/−) relative to the levels seen in wild-type littermates.

been observed for the *Gli* family of transcription factors. The loss of *Gli3* had no observable dental phenotype, whereas the loss of *Gli2* resulted in relatively mild abnormalities in maxillary incisor development (10). However, in *Gli2/Gli3* double mutants there was no normal tooth development with apparent arrest at the early bud (incisors) or prebud stages (molars). Given this redundancy in *Dlx* and *Gli* family members, it will be of interest to determine whether the *Nfic*^{−/−} phenotype is affected by loss of other NFI genes.

Compared to the study of early tooth development described above, few molecules are known to be required for late events in tooth morphogenesis, including root formation. For example, although *Msx-1* is essential for early tooth bud formation, transplantation and rescue studies have shown that *Msx-1* is not essential for later cap and crown formation but appears to again play a role in the long-term survival of odontoblasts and dental pulp (1). Thus, it is difficult to predict which, if any, of the genes identified as essential for early tooth development function in molar root formation. Two mutations, Tabby (*Ta*) and Downless (*Dl*), are known to affect late tooth development (32). However, these mutations affect both molar crown and root formation, whereas the *Nfic*^{−/−} mutation affects predominantly root formation. Since *Nfic* is expressed during both

respectively, showing the expression of *Nfic* in root odontoblasts (arrowhead), preodontoblasts (arrow), periodontal ligament (p), and bone (b) in panel G. Similar expression of *Nfic* was seen in mandibular molars at this stage (not shown).

molar crown and root formation (Fig. 7), while the major phenotype we see is restricted to root formation (Fig. 3 to 6), it will be of interest to determine whether one of the other NFI genes compensates for the loss of *Nfic* during crown formation.

Molar root development begins at ~P9 by outgrowth of a collar of cells (Hertwig's epithelial root sheath) from the molar crown. These epithelial cells then induce the differentiation of dental papillary mesenchymal cells into odontoblasts which, through migration, dentin deposition, and mineralization form the hard structure of the root. Our data suggest that this collar of cells either fails to grow out of the crown and/or fails to induce odontoblast differentiation (Fig. 5). Whether this molar root defect is related mechanistically to the abnormal incisor development seen in the *Nfic*$^{-/-}$ mice is unclear. However, it is intriguing that the maxillary incisor defects seen in *Nfic*$^{-/-}$ mice appear to be due to a failure of differentiation and/or dentin formation in lingual regions of the incisor (Fig. 4F, arrow), much as root formation requires appropriate differentiation and dentin formation at the base of the molar (Fig. 5). Unfortunately, there are no genes or signaling pathways known to be expressed solely in the epithelial root sheath, and the incisors' cellular homologue of the molar root sheath has not been well characterized. In addition, since incisors continue to grow throughout adult life, whereas molar root and crown development and growth terminate, it is possible that there are incisor-specific mechanisms that allow for continuous growth. It will be important to define gene expression patterns in the affected regions of both the molars and incisors in the *Nfic*$^{-/-}$ mice to determine whether these defects are due to changes in similar regulatory pathways. The *Nfic*$^{-/-}$ mouse should provide a unique and important resource to determine the transcriptional and cell-signaling pathways essential for molar root formation.

Given the previously noted widespread expression of *Nfic* during development (3), it is perhaps surprising that the phenotype of the *Nfic*$^{-/-}$ mouse is so restricted. Indeed, most other mouse mutations affecting tooth development also affect other developmental programs, including hair follicle and skin formation (*Ta* and *Dl*), bone formation (*Msx1* and *-2*), craniofacial development (*Msx1* and *-2*, *Pax9*), cardiac development (*Msx1*), and others. However, some of these genes are expressed in migrating neural crest cells that populate many organ systems, which most likely explains their pleiotropic phenotypes (2, 6). Detailed genetic analysis of *Nfic* interactions with other genes will be important in determining whether *Nfic* functions in other organ systems. Also, since a number of human dental and craniofacial defects appear to be due to mutations in human homologues of murine tooth development genes (11, 28, 34), it will be important to determine whether mutations in *NFIC* underlie any of the uncharacterized odontogenic syndromes.

The defects seen here are in striking contrast to the neuro-anatomical defects present in *Nfia*$^{-/-}$ animals (agenesis of the corpus callosum, hydrocephalus, etc. [4]) and the lung defects seen in *Nfib*$^{-/-}$ animals (9) and indicate that these three NFI family members each have unique and essential roles in mouse development. The apparent lack of compensatory changes in the other NFI family members in both *Nfic* (Fig. 8) and *Nfia*$^{-/-}$ mice suggest that there is little if any "feedback" between the family members. This is surprising because there is frequently overlapping expression of the different family members during development (3). However, although the three phenotypes are very different, it is possible that similar changes in transcriptional pathways underlie the anatomical defects seen in all three mutants. We are currently taking two approaches to finding out whether *Nfic* and *Nfia* interact in similar transcriptional and developmental pathways in mice: (i) we are generating *Nfia*/*Nfic* double-knockout mice to assess their phenotype and (ii) we are assessing the earliest changes in gene expression patterns in the affected tissues of *Nfic*$^{-/-}$ and *Nfia*$^{-/-}$ mice to determine the pathways disrupted in each animal. These approaches should help us to understand the pathways underlying the anatomical defects seen in these animals and allow us to determine whether these two NFI genes share common regulatory mechanisms in mice.

## REFERENCES

1. **Bei, M., K. Kratochwil, and R. L. Maas.** 2000. BMP4 rescues a non-cell-autonomous function of Msx1 in tooth development. Development **127:** 4711–4718.
2. **Chai, Y., X. Jiang, Y. Ito, P. Bringas, Jr., J. Han, D. H. Rowitch, P. Soriano, A. P. McMahon, and H. M. Sucov.** 2000. Fate of the mammalian cranial neural crest during tooth and mandibular morphogenesis. Development **127:**1671–1679.
3. **Chaudhry, A. Z., C. E. Lyons, and R. M. Gronostajski.** 1997. Expression patterns of the four nuclear factor I genes during mouse embryogenesis indicate a potential role in development. Dev. Dyn. **208:**313–325.
4. **das Neves, L., C. Duchala, F. Godinho, M. Haxhiu, C. Colmenares, W. Macklin, C. Campbell, K. Butz, and R. Gronostajski.** 1999. Disruption of the murine nuclear factor I-A gene (*Nfia*) results in perinatal lethality, hydrocephalus and agenesis of the corpus callosum. Proc. Natl. Acad. Sci. USA **96:**11946–11951.
5. **Dassule, H. R., P. Lewis, M. Bei, R. Maas, and A. P. McMahon.** 2000. Sonic hedgehog regulates growth and morphogenesis of the tooth. Development **127:**4775–4785.
6. **Ferguson, C. A., A. S. Tucker, and P. T. Sharpe.** 2000. Temporospatial cell interactions regulating mandibular and maxillary arch patterning. Development **127:**403–412.
7. **Fletcher, C. F., N. A. Jenkins, N. G. Copeland, A. Z. Chaudhry, and R. M. Gronostajski.** 1999. Exon structure of the nuclear factor I DNA-binding domain from *Caenorhabditis elegans* to mammals. Mamm. Genome **10:**390–396.
8. **Gronostajski, R. M.** 2000. Role of NFI/CTF gene family in transcription and development. Gene **249:**31–45.
9. **Grunder, A., T. T. Ebel, M. Mallo, G. Schwarzkopf, T. Shimizu, A. E. Sippel, and H. Schrewe.** 2002. Nuclear factor I-B (Nfib)-deficient mice have severe lung hypoplasia. Mech. Dev. **112:**69–77.
10. **Hardcastle, Z., R. Mo, C. C. Hui, and P. T. Sharpe.** 1998. The Shh signaling pathway in tooth development: defects in Gli2 and Gli3 mutants. Development **125:**2803–2811.
11. **Headon, D. J., S. A. Emmal, B. M. Ferguson, A. S. Tucker, M. J. Justice, P. T. Sharpe, J. Zonana, and P. A. Overbeek.** 2001. Gene defect in ectodermal dysplasia implicates a death domain adapter in development. Nature **414:** 913–916.
12. **Hooper, M., K. Hardy, A. Handyside, S. Hunter, and M. Monk.** 1987. HPRT-deficient (Lesch-Nyhan) mouse embryos derived from germline colonization by cultured cells. Nature **326:**292–295.
13. **Kettunen, P., J. Laurikkala, P. Itaranta, S. Vainio, N. Itoh, and I. Thesleff.**

2000. Associations of FGF-3 and FGF-10 with signaling networks regulating tooth morphogenesis. Dev. Dyn. **219:**322–332.

14. **Kruse, U., F. Qian, and A. E. Sippel.** 1991. Identification of a fourth nuclear factor I gene in chicken by cDNA cloning: NFIX. Nucleic Acids Res. **19:** 6641.

15. **Kruse, U., and A. E. Sippel.** 1994. Transcription factor nuclear factor I proteins form stable homo- and heterodimers. FEBS Lett. **348:**46–50.

16. **Lyons, G., M. Ontell, R. Cox, D. Sassoon, and M. Buckingham.** 1990. The expression of myosin genes in developing skeletal muscle in the mouse embryo. J. Cell Biol. **111:**1465–1476.

17. **Mansour, S. L., K. R. Thomas, and M. R. Capecchi.** 1988. Disruption of the proto-oncogene *int-2* in mouse embryo-derived stem cells: a general strategy for targeting mutations to non-selectable genes. Nature **336:**348–357.

18. **Meisterernst, M., L. Rogge, C. Donath, I. Gander, F. Lottspeich, R. Mertz, T. Dobner, and R. Fockler.** 1988. Isolation and characterization of the porcine nuclear factor I (NFI) gene. FEBS Lett. **236:**27–32.

19. **Nagata, K., R. Guggenheimer, T. Enomoto, J. Lichy, and J. Hurwitz.** 1982. Adenovirus DNA replication in vitro identification of a host factor that stimulates synthesis of the preterminal protein-dCMP complex. Proc. Natl. Acad. Sci. USA **79:**6438–6442.

20. **Nagata, K., R. A. Guggenheimer, and J. Hurwitz.** 1983. Specific binding of a cellular DNA replication protein to the origin of replication of adenovirus DNA. Proc. Natl. Acad. Sci. USA **80:**6177–6181.

21. **Peters, H., A. Neubuser, K. Kratochwil, and R. Balling.** 1998. Pax9-deficient mice lack pharyngeal pouch derivatives and teeth and exhibit craniofacial and limb abnormalities. Genes Dev. **12:**2735–2747.

22. **Qiu, M., A. Bulfone, I. Ghattas, J. J. Meneses, L. Christensen, P. T. Sharpe, R. Presley, R. A. Pedersen, and J. L. Rubenstein.** 1997. Role of the Dlx homeobox genes in proximodistal patterning of the branchial arches: mutations of Dlx-1, Dlx-2, and Dlx-1 and -2 alter morphogenesis of proximal skeletal and soft tissue structures derived from the first and second arches. Dev. Biol. **185:**165–184.

23. **Rupp, R., U. Kruse, G. Multhaup, U. Gobel, K. Beyreuther, and A. Sippel.** 1990. Chicken NFI/TGGCA proteins are encoded by at least three independent genes: NFI-A, NFI-B and NFI-C with homologues in mammalian genomes. Nucleic Acids Res. **18:**2607–2616.

24. **Santoro, C., N. Mermod, P. Andrews, and R. Tjian.** 1988. A family of human CCAAT-box-binding proteins active in transcription and DNA replication: cloning and expression of multiple cDNAs. Nature **334:**218–224.

25. **Sarkar, L., M. Cobourne, S. Naylor, M. Smalley, T. Dale, and P. T. Sharpe.** 2000. Wnt/Shh interactions regulate ectodermal boundary formation during mammalian tooth development. Proc. Natl. Acad. Sci. USA **97:**4520–4524.

26. **Soriano, P., C. Montgomery, R. Geske, and A. Bradley.** 1991. Targeted disruption of the c-*src* proto-oncogene leads to osteopetrosis in mice. Cell **64:**693–702.

27. **St Amand, T. R., Y. Zhang, E. V. Semina, X. Zhao, Y. Hu, L. Nguyen, J. C. Murray, and Y. Chen.** 2000. Antagonistic signals between BMP4 and FGF8 define the expression of Pitx1 and Pitx2 in mouse tooth-forming anlage. Dev. Biol. **217:**323–332.

28. **Stockton, D. W., P. Das, M. Goldenberg, R. N. D'Souza, and P. I. Patel.** 2000. Mutation of PAX9 is associated with oligodontia. Nat. Genet. **24:**18–19.

29. **Thesleff, I., and P. Sharpe.** 1997. Signalling networks regulating dental development. Mech. Dev. **67:**111–123.

30. **Thomas, B. L., A. S. Tucker, M. Qui, C. A. Ferguson, Z. Hardcastle, J. L. Rubenstein, and P. T. Sharpe.** 1997. Role of Dlx-1 and Dlx-2 genes in patterning of the murine dentition. Development **124:**4811–4818.

31. **Tucker, A. S., A. Al Khamis, and P. T. Sharpe.** 1998. Interactions between Bmp-4 and Msx-1 act to restrict gene expression to odontogenic mesenchyme. Dev. Dyn. **212:**533–539.

32. **Tucker, A. S., D. J. Headon, P. Schneider, B. M. Ferguson, P. Overbeek, J. Tschopp, and P. T. Sharpe.** 2000. Edar/Eda interactions regulate enamel knot formation in tooth morphogenesis. Development **127:**4691–4700.

33. **van Genderen, C., R. M. Okamura, I. Farinas, R. G. Quo, T. G. Parslow, L. Bruhn, and R. Grosschedl.** 1994. Development of several organs that require inductive epithelial-mesenchymal interactions is impaired in LEF-1-deficient mice. Genes Dev. **8:**2691–2703.

34. **Wilkie, A. O., Z. Tang, N. Elanko, S. Walsh, S. R. Twigg, J. A. Hurst, S. A. Wall, K. H. Chrzanowska, and R. E. Maxson, Jr.** 2000. Functional haploinsufficiency of the human homeobox gene MSX2 causes defects in skull ossification. Nat. Genet. **24:**387–390.